Geometrically induced π-band splitting in graphene superlattices*

Yanpei Wei(魏艳佩), Tiantian Jia(贾甜甜), and Gang Chen(陈刚)†

Department of Physics, University of Jinan, Jinan 250022, *China*

(Received 25 August 2016; revised manuscript received 20 November 2016; published online 10 January 2017)

According to band folding analyses, the graphene superlattices can be differed by whether the Dirac points are folded to Γ point or not. In previous studies, the inversion symmetry preserved defects open bandgap in the former superlattices while they cannot in the latter ones. In this paper, by using density functional theory with generalized gradient approximation, we have carefully studied the electronic properties of the latter graphene superlattices, in which the defects would induce π-band splitting to get the π_{a1}–π_{a2} and π_{z1}–π_{z2} band sets. Based on our detailed studies, such splitting could be attributed to the geometrically induced bond-symmetry breaking. In addition, these band sets could be shifted toward each other by the methodology of strain engineering. A bandgap would be opened once the band sets start to overlap. Then, its gap width could be continuously enlarged by enhancing strain until reaching the maximum value determined by the defect density. These studies contribute to the bandstructure engineering of graphene-based nanomaterials, which would be interesting to call for further investigations on both theory and experiment.

Keywords: first-principles calculation, novel two-dimensional nanostructure, bandgap opening and tuning

PACS: 81.05.Zx, 81.05.Rm, 81.05.ue **DOI:** 10.1088/1674-1056/26/2/028103

1. Introduction

Since its discovery in 2004,[1] graphene has attracted intensive attention owe to its unique properties attributed to the intersection of the π-type electronic bands occurring at the corners of its hexagonal Brillouin zone, which forms the so-called Dirac cones in the proximity around K and K' points to make graphene as a semimetal. The linear dispersion relationship around Dirac point makes charge carriers as high mobility massless Fermions which could be also continuously tuned between electrons and holes, showing attractive application potential in next-generation high-performance photoelectronics. On the other hand, the band closure properties of graphene would however hinder its usage in advanced nanodevices which usually require a high on/off ratio. Hence, considerable attempts have been made to open a bandgap in graphene. The functional group adsorption, interface interaction in heterostructures and the substrate supported graphene, substitution doping, size effects in nanoribbons, and the structural defects, etc. have been shown effectively in modifying electronic properties of two-dimensional nanostructures.[2–20] Among these studies, the most often discussed bandgap opening mechanisms are the sublattice equivalence breaking, quantum confinement, and chemical perturbation to the sp^2 electronic configuration.

Recently, Bai *et al.* investigated the nicely patterned graphene nanomesh fabricated by using the block copolymer lithography.[12] The techniques of the nanoimprint lithography, the block-copolymer self-assembly for high-resolution nanoimprint template, and the cylinder-forming diblock copolymer templates have also been proved to be efficient in patterning graphene nanomeshes.[13,14] Also, a most recent work shows the possibilities in preparing graphene nanomesh with the well-controlled patterns and vacancy hole shapes by combining the e-beam lithography and the oxygen reactive ion etching.[15] These experimental progresses in fabricating advanced nanomaterials suggest the possibilities in producing graphene nanomesh with nice precision. The periodically arranged antidots impose new Born-von Karman boundary conditions to make the graphene as superlattice.[21] Motivated by the experimental studies, the bandgap opening in the inversion symmetry preserved (ISP) graphene superlattices were investigated in our previous studies.[3,4] In some superlattices, the Dirac cones of pristine graphene can be folded to Γ point forming four-fold degeneracy. The ISP defects would open bandgap to make graphene semiconducting. For the other superlattices in which the Dirac points still remain two-fold degenerate, the ISP defects would however not alter their semimetal nature. Up to now, the latter superlattices are still less of studies due to their band closure properties. In fact, the ISP defects would induce the π-band splitting in all of the graphene superlattices no matter whether the Dirac cone would be folded to Γ point or not. So, a question could be raised: why would the π-band splitting make some graphene superlattices to be semiconducting while it would not for the other ones? In order to answer this question, we have studied the geometrically induced π-band splitting in graphene super-

*Project jointly supported by the Natural Science Foundation of Shandong Province (Grant NO. TSHW20101004) and the National Natural Science Foundation of China (Grant Nos. 11374128 and 11674129).

†Corresponding author. E-mail: phdgchen@163.com

© 2017 Chinese Physical Society and IOP Publishing Ltd

lattices in detail in this paper. Based on our studies, we found that the positions of the split intervals in energy would in fact determine the bandgap opening or not. A comprehensive discussion on the origin of the π-band splitting has also been made as a contribution to the bandgap opening mechanism studies. Unlike the superlattices with Dirac cone being folded to Γ point, the other superlattices have the split intervals in energy to be laid above or below the Fermi level leaving the semimetal nature unaffected. Interestingly, they could however be shifted toward each other by applying uniaxial strain to open a bandgap once they start to overlap at the Fermi level.

2. Computational details

Our spin-polarized first-principles studies were carried out by using the Vienna *ab initio* simulation package within the framework of density functional theory.[22] The plane wave basis and the projector augmented-wave potential were adopted.[23] The exchange and correlation energy was calculated by using the generalized gradient approximation with the Perdew and Wang (PW91) formalism.[24] The solution of the Kohn–Sham equation was calculated by an efficient matrix diagonalization technique based on a sequential band-by-band residual minimization method.[22] A cutoff energy of 400 eV was used for the planewave basis set to expand the wavefunction. For the electronic property integration, the Monkhorst–Pack technique[25] was used to sample k points. A supercell with 15 Å vacuum along Z direction was used to model the sheet material with graphene superlattice being placed in XY plane. For the studies using the primitive unit cell and the smallest rectangle unit cell, we calculated the electronic properties with a $15\times15\times1$ k-mesh. The in plane lattices of the hexagonal primitive unit cell were calculated to be 2.47 Å. For superlattices, the corresponding unit cells of 12.8 Å$\times$12.3 Å$\times$15 Å and 34.2 Å$\times$19.7 Å$\times$15 Å were adopt. Therefore, the k-meshes of $7\times7\times1$ and $3\times5\times1$ were respectively used in the studies. The electronic properties were converged to 10^{-5} eV and the Hellmann–Feynman forces on each atom were optimized to reach 0.01 eV/Å.

3. Results and discussion

In the experimentally fabricated nanomeshes, the defects are often hexagonally or orthogonally arranged in graphene. To facilitate discussion of the uniaxial strain effects, we would like to concentrate on studying the orthogonally patterned superlattices, whose conclusions could shed light on the hexagonal ones. As shown in Fig. 1(a), the smallest orthogonal unit could be defined by $\boldsymbol{A}_1 = \boldsymbol{a} + \boldsymbol{b}$ and $\boldsymbol{B}_1 = -\boldsymbol{a} + \boldsymbol{b}$, where $\boldsymbol{a}$ and $\boldsymbol{b}$ are the basis lattices of the primitive unit cell. Its rectangular Brillouin zone (r-BZ) is shown in Fig. 1(b) along with the hexagonal one (h-BZ) for the primitive unit cell. Clearly, one can see that the K point in the h-BZ is now folded to the T_1 ($\frac{2}{3}\boldsymbol{\Gamma}_1\boldsymbol{Y}_1$) point in the r-BZ. This can also be seen in the calculated band structure as presented in Fig. 1(c). Hereafter, in comparison with the graphene studied with the primitive unit cell, we would like to refer the one studied with the orthogonal supercell $\boldsymbol{A}\times\boldsymbol{B}$ with $\boldsymbol{A} = P\boldsymbol{A}_1$ and $\boldsymbol{B} = Q\boldsymbol{B}_1$ as (P,Q) pseudo graphene superlattice (PGS). Thus, the smallest orthogonal lattice shown in Fig. 1(a) corresponds to the (1,1) PGS. In Fig. 1, the (1,2) and (1,3) PGSes are also presented. The K point in h-BZ of the primitive unit cell is now folded to the T_2' for the (1,2) PGS and the Γ point for the (1,3) PGS. Based on our careful analysis, the studied (P,Q) PGSes could be sorted into $Q = 3q$, $3q+1$, and $3q+2$ (q is integer) groups to facilitate discussion, which have the Dirac point K of the primitive unit cell being folded to the Γ, $\frac{2}{3}\boldsymbol{\Gamma Y}$, and $\frac{2}{3}\boldsymbol{\Gamma Y}'$ points of the corresponding supercells, respectively. Introducing a defect in the supercell would impose new Born-von Karman boundary conditions to pattern the real graphene superlattice.[21]

Previous studies have shown that the ISP defect, such as the D_{6h} antidot, can open bandgap in $3q$ superlattices at Dirac point making them semiconducting, while it could not alter the semimetal nature of the $3q+1$ and $3q+2$ superlattices.[3,4] In these papers, the studied D_{6h} antidots correspond to the vacancy defects generated by removing the carbon nanoflakes which have D_{6h} point group symmetry to keep the inversion symmetry in the defected graphene. In fact, the π-band splitting also happens in the semimetal superlattices, whose split energy intervals are however apart away the Fermi level to leave the band closure properties unaffected. In Fig. 2, we have studied the (3,5) PGS. In the band structure figure, the bands close to the Fermi level are marked by π_a and π_z at Y point, whose band decomposed charge densities are studied in detail. As presented in Fig. 2, the anisotropic distribution shows that the band characters of π_a and π_z bands respectively correspond to the bonds along armchair and zigzag directions. The band closing Dirac point is located at $\frac{2}{3}\boldsymbol{\Gamma Y}$ point. Now, with the purpose to examine the band splitting, we have carried out detailed studies on its electronic properties after introducing a hexagonal defect in the repeated unit. For the previously studied antidot, the π-electron wavefunction will be terminated on the edge of the vacancy hole to act as an infinite high potential wall to block the electron wave from propagating, which may bear the effects from the wavefunction termination as well as the periodic perturbation on the π-electron potential.

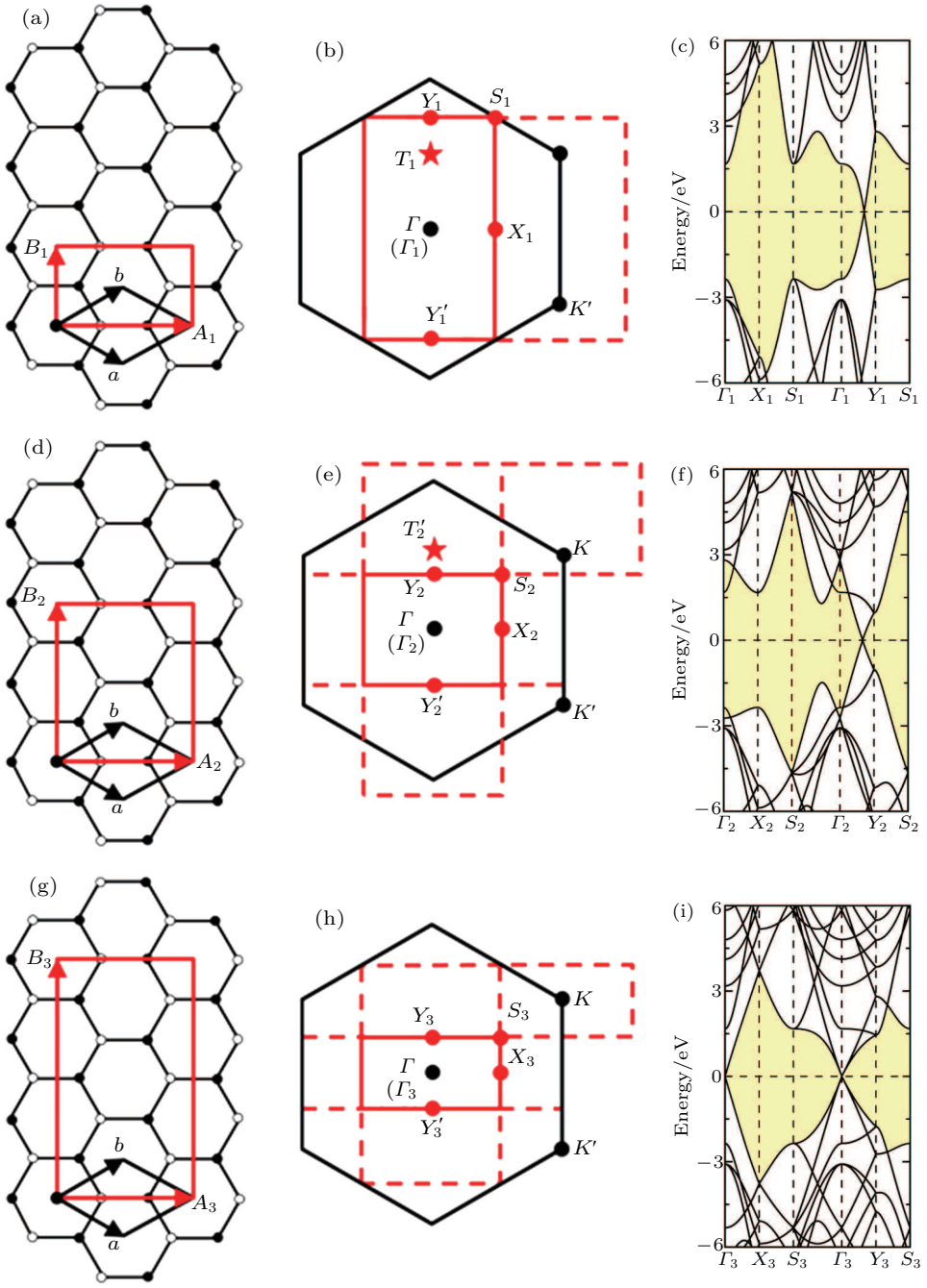


Fig. 1. (color online) The schematic structure (a), Brillouin zone (b), and band structure (c) for the (1,1) PGS; those for the (1,2) PGS are in panels (d), (e), and (f); and the ones for the (1,3) PGS are in panels (g), (h), and (i).

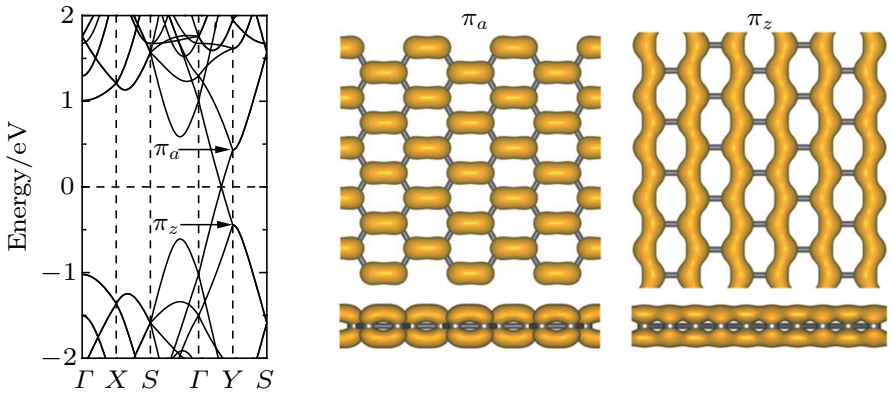


Fig. 2. (color online) The calculated band structure of the (3,5) PGS. The band decomposed charge densities for the bands along ΓY path as marked by π_a and π_z are studied at Y point with the iso-value of 0.01 e/Å^3. Both top and side views are shown.

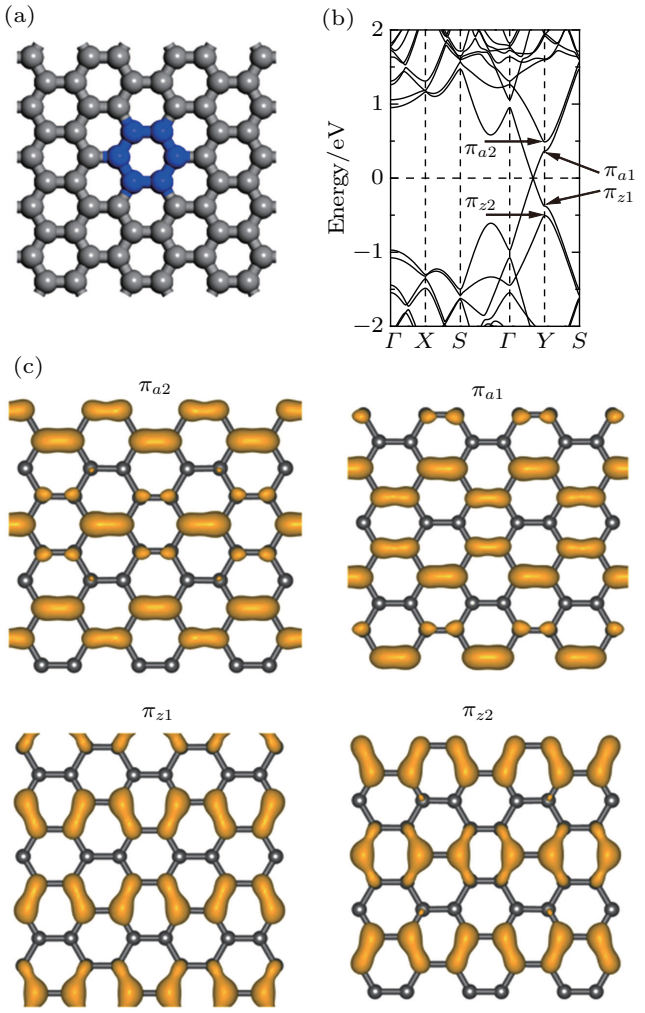


Fig. 3. (color online) (a) The schematic structure for the D_{6h} defect introduced by contracting the highlighted C_6 hexagon. (b) The band structure for the (3,5) superlattice patterned by such defect. The split bands along ΓY path are marked with π_{a1}, π_{a2}, π_{z1}, and π_{z2} at Y point. (c) The band decomposed charge densities at iso-value of 0.01 e/Å^3 for the split bands.

In order to solely examine the effects of the periodic perturbation on the potential, we would like to follow the idea of introducing a periodic potential to the graphene to rule out the effects from the wavefunction termination. A defect in the repeated unit by contracting a C_6 hexagon is introduced to perturb the potential which is schematically shown in Fig. 3(a). Here, it is contracted of $\sim 3\%$ to enhance the corresponding C–C transfer integral according to the methodology of tight-binding (TB).[21] The atoms of this C_6 hexagon are fixed while the rest atoms are fully relaxed. After structural optimization, the electronic properties are carefully studied. In Fig. 3(b), the energy band structure is presented. Compared to the band structure shown in Fig. 2 for the defect free lattice, some changes have happened though the semimetal nature remains unaffected. Especially, there are band splittings happened to the π-type bands at both Y and Γ points. For the fact that the split intervals at Y point are closer to the Fermi level in band energy, we would concentrate on studying the Y-point band splitting in this paper, whose conclusions could shed light on the Γ-point band splitting. In Fig. 3(b), the π_a band at Y point would split into the $\pi_{a1} - \pi_{a2}$ band set with an energy interval E_a. Similar splitting happens also to the π_z band with an energy interval E_z ($E_z = E_a$). According to the methodology of TB, the main characteristics of the band structure of graphene could be got by considering only the nearest neighboring atoms.[21] For a given atom, the overlap between its atomic orbitals and the ones of its nearest atoms dominates the transfer integral between them. The slight change of the interatomic distances between them could affect the overlap of the corresponding atomic orbitals, which would in turn alter the corresponding transfer integral accordingly. The C–C bond contraction of $\sim 3\%$ in the highlighted C_6 hexagon (see Fig. 3(a)) could enhance the corresponding transfer integrals by $\sim 10\%$ accordingly.[21,26] In our previous studies of the $3q$ graphene superlattices, the TB calculations were found to support our first-principles calculations in bandgap opening at Γ point.[3] Unfortunately, we ignored the band splitting phenomena in the $3q+1$ and $3q+2$ superlattices previously.

In Fig. 4, the band structures calculated with the TB method for the defect-free (3,5) PGS and the defect-patterned (3,5) superlattice are shown. The defect was mimicked by enhancing the transfer integrals by 10% of the C–C bonds in the C_6 hexagon (see the highlighted C_6 hexagon in Fig. 3(a)). Compared to the Fig. 3(b), the TB method agrees very well with the first-principles method on the π-band splitting phenomena at Y point, etc. By projecting the wavefunctions, the band decomposed charge densities of the split π_{a1}, π_{a2}, π_{z1}, and π_{z2} bands are studied in Fig. 3(c), suggesting the different changes happened to the corresponding bonds, respectively. Hereafter, we would like to refer these bonds as π_{a1}, π_{a2}, π_{z1}, and π_{z2} bonds to facilitate discussion. In the defect free graphene, the C–C bonds are almost the same in length, which are calculated to be 1.42 Å. After introducing the C_6-defect in the repeated unit, we have performed full structural optimization. Except for the C_6 hexagon, all of the other C atoms are free to relax. After the optimization, we have again measured the bond lengths. As compared to the 1.42 Å bond length of the defect free graphene, all the π_{a1} and π_{z2} bonds now get shorter overall while all the π_{a2} and π_{z1} bonds get longer overall. On average, the bond lengths are shortened by about 0.48% and 0.72% for the π_{a1} and π_{z2} bonds while they are elongated by about 0.45% and 0.62% for the π_{a2} and π_{z1} bonds, respectively. The bond length changes hint the different alternations of the corresponding C–C transfer integrals, which would then alter the corresponding band energies accordingly to account for the π-band splitting.

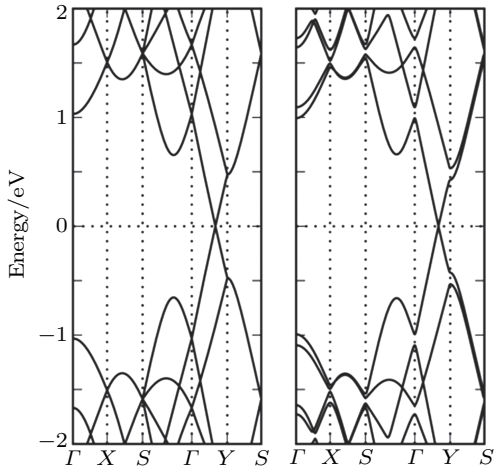


Fig. 4. The electronic band structures calculated with TB method for the defect-free (3,5) PGS (the left) and the defect-patterned (3,5) superlattice (the right). The defect was mimicked by enhancing the transfer integrals of the C–C bonds in the C_6 hexagon as highlighted in Fig. 3(a).

In the $3q$ type superlattices, the opposite Dirac cones would be folded onto Γ point. The ISP defects could then open bandgap by lifting the four-fold degeneracy.[3,4] In the spirit of the concept of pseudo spin, the bandgap opening in $3q$-type graphene superlattices may be understood by the intervalley scattering. The periodically arranged defects could be approximately treated as introducing a periodic perturbation potential $V_{\rm d}(\boldsymbol{r})$ to the pristine graphene. If the wavevectors of the opposite $\boldsymbol{D}$ and $\boldsymbol{D}'$ valleys (the positions of the opposite Dirac cones) differ with each other by a reciprocal lattice $\boldsymbol{G}$ or mach with each other at a same point, the intervalley scattering would induce band splitting. Unlike the $3q$-type superlattices, in the $(3q+1)$- and $(3q+2)$-type superlattices, the wavevector between two nearest opposite Dirac points is $\frac{2}{3}\boldsymbol{\Gamma Y}$ failing to satisfy the above mentioned conditions for intervalley scattering. Based on our analysis of the bond length change in the defected graphene, we would like to refer the 3-fold homogeneous equivalence of the C–C honeycomb bonding configuration in graphene as bond symmetry. Then, the band splitting happened in the free standing ISP-defect patterned superlattices could be attributed to the bond symmetry breaking, which alters the related transfer integrals to change the corresponding band energies. As in the case of the lattice studied in Fig. 3(b), the bond symmetry breaking splits the degenerate π_a and π_z bands into π_{a1}–π_{a2} and π_{z1}–π_{z2} band sets with split energy intervals E_a and E_z, respectively. Actually, similar bond symmetry breaking also happens in the $3q$-type superlattices, in which the E_a and E_z are totally overlapped at Γ point to account for the bandgap opening.

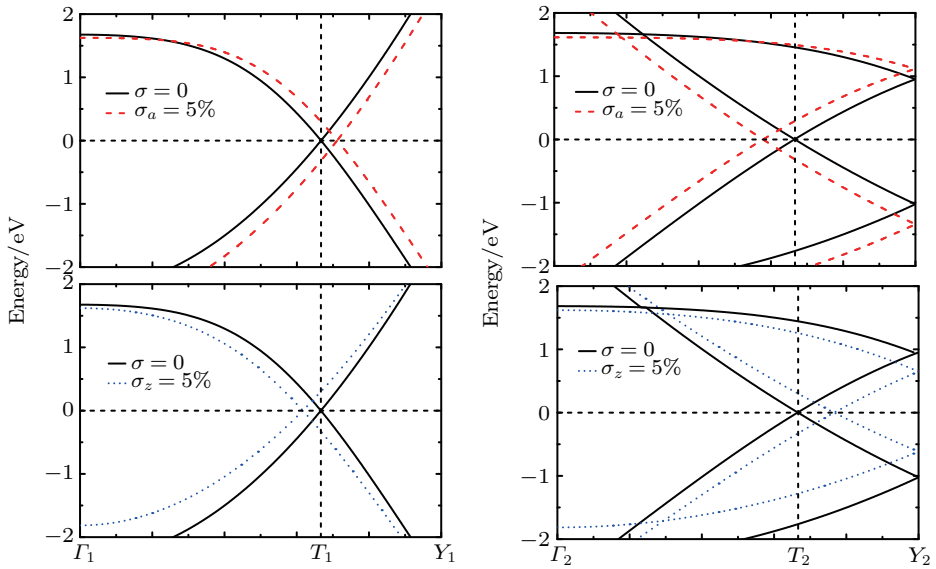


Fig. 5. (color online) The Dirac point shifts induced by the uniaxial strain in the (1,1) and (1,2) PGSes are presented in the left and right panels, respectively.

Now, we reach the conclusions: (i) the π-bands at Y point can be split to gain energy intervals which are however apart away the Fermi level, and (ii) the band closing Dirac points remain unaffected at the type points. So, an interesting question could be raised: could the Dirac point be moved to Y point to check the cooperative effects of the Dirac point shift and the π-band splitting on the band structure engineering of graphene? Fortunately, this could be realized by applying uniaxial strain. We have carefully examined the effects of the uniaxial strain σ_a applied along the armchair lattice ($\boldsymbol{A}$ lattice) and the σ_z applied along the zigzag lattice ($\boldsymbol{B}$ lattice), respectively. In the process of enhancing strain, the Dirac point has been found to continuously move along ΓY path in the corresponding r-BZ. We use the (1,1) ($3q+1$ type) and (1,2) ($3q+2$ type) PGSes as prototypes to illustrate the strain effects in Fig. 5, respectively (The strain is accounted by the change of

the corresponding lattice). The σ_a strain would shift the Dirac point along ΓY path toward Y point for the (1,1) and the Γ point for the (1,2) PGSes, respectively. The calculated results under 5% uniaxial strains are shown in Fig. 5. Compared to the free-standing graphene, the studied uniaxial strain σ_z (σ_a) would elongate the C–C bonds along zigzag (armchair) direction while it only slightly shortens the corresponding bonds along armchair (zigzag) direction, resulting in bond symmetry breaking of the ideal sp^2 configuration. The transfer integrals of elongated bonds would be weakened to increase the corresponding band energy, while the slightly contracted bonds would get enhanced to gain lower band energy accordingly, accounting for the Dirac point shift along ΓY path. In fact, the similar results on Dirac point shift owe to the perturbation on the ideal sp^2 configuration were also discussed in the previous studies of the uniaxial strain engineered graphene and the $(3n,0)$ ($n = 3, 4, 5, 6$) single-walled carbon nanotubes.[27,28]

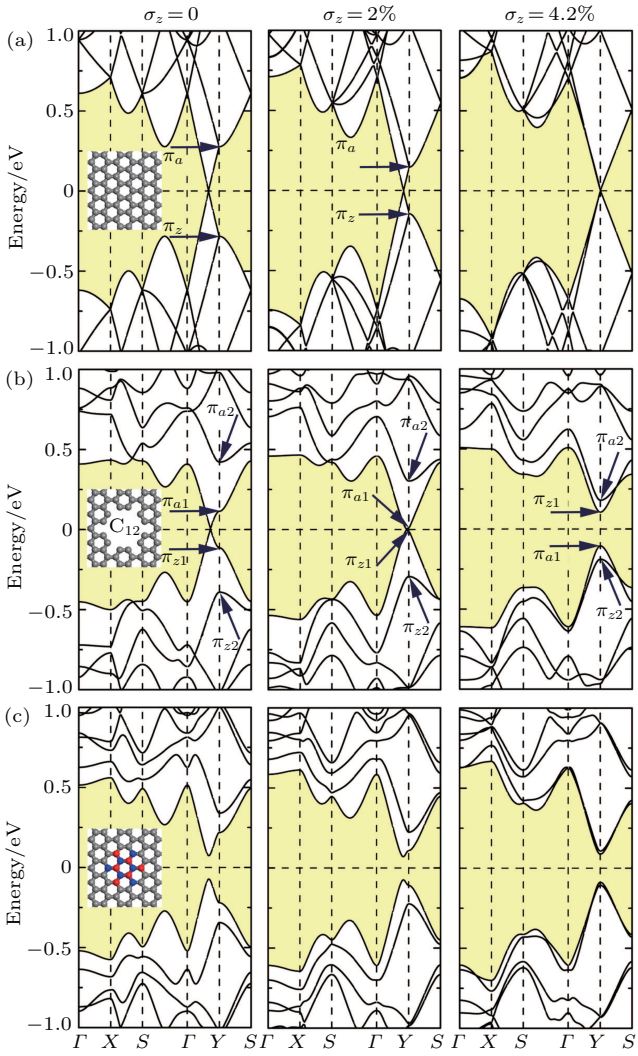


Fig. 6. (color online) The bandstructure of the uniaxial strain σ_z engineered (8,8) superlattice. The (a), (b), and (c) are for the defect free PGS, C_{12} antidot patterned superlattice, and $(BN)_6$ nanoflake patterned superlattice, respectively.

With the purpose to shed light on the experimentally investigated graphene nanomeshes, we have also studied the ISP vacancy hole patterned graphene superlattices. In Fig. 6, the σ_z strain engineered (8,8) graphene superlattice patterned by regularly arranged D_{6h} C_{12} antidots has been carefully analyzed in detail as a prototype. Here, the notation of C_n accounts for the antidot formed by removing a n-atom D_{6h} carbon nanoflake from the graphene (the vacancy hole edge is passivated by hydrogen). As shown in Fig. 6(a) for the (8,8) PGS, the Dirac point would be continuously moved toward Y point along with strain enhancing until it arrives at Y point under $\sigma_z = 4.2\%$. In Fig. 6(b), we have studied the cooperative effects of the defect induced π-band splitting and the uniaxial strain induced Dirac point shift for the C_{12} antidot patterned (8,8) superlattice. Besides of the experimental fact of the successful fabrication of vacancy hole patterned graphene superlattice, we have performed the *ab initio* molecular dynamics simulations to evaluate the stability of the C_{12} patterned superlattice. The simulations have been performed at the temperatures of 1000 K and 1500 K, which last for 6 ps with the time step of 1 fs. The structure can sustain in our simulations, implying that this superlattice structure is separated by high-energy barriers from other local minima on the potential energy surface. After introducing C_{12} antidot in the unit cell, the free standing (8,8) superlattice gets the split $\pi_{a1} - \pi_{a2}$ and $\pi_{z1} - \pi_{z2}$ band sets with the energy intervals E_a and E_z of ~ 0.29 eV. The band splitting intervals are in fact the intrinsic characters of the defected superlattice, which is determined by the defect itself and the defect density in the graphene. The ~ 0.29 eV gap width of the studied (8,8) superlattice is found to keep almost constant during the uniaxial strain loading. By applying the σ_z strain, its Dirac point would be shifted away $\frac{2}{3}\Gamma Y$ point toward the Y point in the (8,8) PGS. The Dirac cone in graphene is actually formed by the band crossing between the π_a- and π_z-type bands. After loading the σ_z strain, the C–C bonds along zigzag direction would be overall elongated while the bonds in armchair direction would be overall shortened. The corresponding band energies of the π_z- and π_a-type bands would gain different energy changes to move the band crossing position, accounting for the Dirac cone shift along the ΓY path. As referring to the Fermi level, in the process of loading σ_z strain, the π_{a1}–π_{a2} band set shown in Fig. 6(b) for the C_{12}-patterned (8,8) superlattice would be moved downward while the π_{z1}–π_{z2} band set would be lifted upward. Under $\sigma_z \sim 2\%$, the π_{a1} and π_{z1} bands get touch with each other at Y point. Then, further increasing the σ_z strain, the energy interval E_a of π_{a1}–π_{a2} band set would start to overlap with the E_z of π_{z1}–π_{z2} band set at Y point. Thus, a bandgap E_{gap} would appear at Fermi level to make the superlattice to be semiconducting, which would get broader in width by en-

hancing the strain unit reaching the maximum E_{max} (equals to E_a and E_z) under $\sigma_z \sim 4.6\%$. The evolution of the E_{gap} as a function of the applied strain has been presented in Fig. 7(a). Upon the $\sigma_z = 4.6\%$, its width starts to decrease again until the π_{a2} and π_{z2} bands start to cross with each other to form new Dirac cone. With the purpose to evaluate the stability of the strain engineered graphene superlattice, we have also carried out *ab initio* molecular dynamics simulations of the C_{12} patterned (8,8) superlattice under the conditions of strain loading, which were previously proved to be useful for evaluating the stability of 2D materials.[29,30] The strain loading of 2% and 4.6% were selected for illustrations in our studies, which are the crucial value for starting to open bandgap and the one for obtaining the maximum gap width. Our simulations lasted for 6 ps with the time step of 1 fs at the temperature of 1500 K. The geometrical structures of the strain engineered (8,8) superlattices were found to remain in our simulations, suggesting good structural stabilities. Using the structures obtained at the end of the simulations, we have also performed full structure optimizations, which could quickly converge to the ideal 2D geometrical structures of the 2% and 4.6% strain engineered (8,8) superlattices, respectively. Besides the $(3q+2)$-type superlattices as illustrated by the (8,8) antidot patterned superlattice, the same phenomena have also been found in our studies of the $(3q+1)$-type superlattices. Furthermore, we have investigated the tuning of the gap maximum E_{max} as a function of the lattice size and presented the results in Fig. 7(b). One can see that the E_{max} could be tuned by controlling the defect density in graphene, showing the possibilities in obtaining proper on/off ratio toward the application demand.

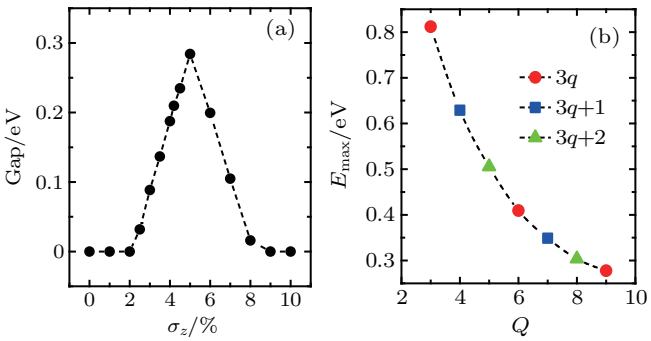


Fig. 7. (color online) (a) The evolution of the bandgap versus the applied strain. (b) The maximum gap width E_{max} of the (8, Q) superlattice as a function of the lattice size Q. The bandgaps of the $3q$-type superlattices are also presented in panel (b) for comparison.

Suggested by the previous studies,[3,4,6–9] the substitution doping of the BN nanoflakes in graphene would be a promising method in opening bandgap in graphene for the practical usage in the field-effect transistors, etc. So, in comparison, we have also calculated the electronic properties of the (8,8) superlattice after patching the C_{12} antidot vacancy holes with $(BN)_6$ nanoflakes. As shown in Fig. 6(c), a bandgap opens for the free standing superlattice due to the sublattice equivalence breaking, suggesting the difference in bandgap opening mechanism as referred to that of the ISP defect patterned superlattice. Though the bandgap could be also shifted along the ΓY path by applying uniaxial strain, the width of ~ 0.15 eV of the $(BN)_6$ nanoflake patched graphene superlattice keeps almost unchanged.

4. Conclusions

We have carefully investigated the geometrically induced π-band splitting of graphene superlattices. The 3-fold homogeneously distributed C–C bonds surrounding each C atom could be sorted into two groups, the bonds along armchair and the ones along zigzag directions, respectively. The band-decomposed charge density analysis shows that the Dirac cone is composed by the π_a/π_z band intersection. The regularly arranged ISP defects induce the π-band splitting to get the π_{a1}–π_{a2} and π_{z1}–π_{z2} band sets with split energy intervals E_a and E_z ($E_z = E_a$), which in fact corresponds to the geometrical symmetry breaking of the 3-fold homogeneous equivalence of the C–C bonds. In the $3q$ superlattices with Dirac cones being folded to Γ point, the E_a and E_z are totally overlapped at the Fermi level to open a bandgap. However, in the other superlattices, they would be respectively above and below the Fermi level. Each of the π_{a1}–π_{a2} and π_{z1}–π_{z2} band sets contribute a band branch to cross with each other at the Fermi level to form Dirac cone, keeping the semimetal nature unaffected. Interestingly, the band sets of these superlattices could be shifted toward each other by applying uniaxial strain, which would induce the semimetal-semiconductor transition once the E_a and E_z start to overlap at the Fermi level. Furthermore, the gap width would be enlarged by enhancing strain to reach its maximum E_{max} which could also be tuned by controlling the defect density in graphene.

Acknowledgment

The authors gratefully acknowledge the computing resources from the University of Jinan. Prof. Zhao P, Dr. Wang H, and Dr. Liu J are highly appreciated for carefully reading through our manuscript.

References

[1] Novoselov K S, Geim A K, Morozov S V, Jiang D, Katsnelson M I, Grigorieva I V, Dubonos S V and Firsov A A 2005 *Nature* **438** 197
[2] Zhou J, Wang Q, Sun Q, Chen X S, Kawazoe Y and Jena P 2009 *Nano Lett.* **9** 3867
[3] Xiu S L, Gong L, Wang V, Liang Y Y, Chen G and Kawazoe Y 2014 *J. Phys. Chem. C* **118** 8174
[4] Xiu S L, Zhemg M M, Zhao P, Zhang Y, Liu H Y, Li S J, Chen G and Kawazoe Y 2014 *Carbon* **79** 646

[5] Agrawal B K and Agrawal S 2013 *Physica E* **50** 102
[6] Sun M, Tang W, Ren Q, Zhao Y, Wang S, Yu J, Du Y and Hao Y 2016 *Physica E* **80** 142
[7] Denis P A, Huelmo C P and Martins A S 2016 *J. Phys. Chem. C* **120** 7103
[8] Nascimento R, Martins J da R, Batista R J C and Chacham H 2015 *J. Phys. Chem. C* **119** 5055
[9] Xu L, Wang L, Huang W, Li X and Xiao W 2014 *Physica E* **63** 259
[10] Chen Z, Lin Y M, Rooks M J and Avouris P 2007 *Physica E* **40** 228
[11] Jia T T, Zheng M M, Fan X Y, Su Y, Li S J, Liu H Y, Chen G and Kawazoe Y 2016 *Sci. Rep.* **6** 18869
[12] Bai J W, Zhong X, Jiang S, Huang Y and Duan X F 2010 *Nat. Nanotechnol.* **5** 190
[13] Kim M, Safrom N S, Han E, Arnold M S and Gopalan P 2010 *Nano Lett.* **10** 1125
[14] Liang X, Jung Y S, Wu S, Ismach A, Olynick D L, Cabrini S and Bokor J 2010 *Nano Lett.* **10** 2454
[15] Liu L Z, Tian S B, Long Y Z, Li W X, Yang H F, Li J J and Gu C Z 2014 *Vacuum* **105** 21
[16] Yang Y, Cao J X and Yang W 2008 *Chin. Phys. B* **17** 1881
[17] Guo Y H, Cao J X and Xu B 2016 *Chin. Phys. B* **25** 017101
[18] Wang H B, Su Y and Chen G 2014 *Chin. Phys. B* **23** 018103
[19] Hu Q K, Wang H Y, Wu Q H, He J L and Zhang G L 2011 *Chin. Phys. Lett.* **28** 126101
[20] Wang J, Duan X M and Zhang P 2016 *Chin. Phys. B* **25** 057301
[21] Singleton J 2001 *Band Theory and Electronic Properties of Solids* (Oxford: Oxford University Press)
[22] Kresse G and Furthmüller J 1996 *Phys. Rev. B* **54** 11169
[23] Kresse G and Joubert D 1999 *Phys. Rev. B* **59** 1758
[24] Perdew J P and Wang Y 1992 *Phys. Rev. B* **45** 13244
[25] Monkhorst H J and Pack J D 1976 *Phys. Rev. B* **13** 5188
[26] Porezg D, Frauenheim Th, Kühler Th, Seifert G and Kaschner R 1995 *Phys. Rev. B* **51** 12947
[27] Choi S M, Jhi S H and Son Y W 2010 *Phys. Rev. B* **81** 081407
[28] Miyake T and Saito S 2005 *Phys. Rev. B* **72** 073404
[29] Li J, Fan X, Wei Y, Wang V and Chen G 2016 *Chem. Phys. Lett.* **660** 244
[30] Li J, Wei Y, Fan X, Wang H, Song Y, Chen G, Liang Y, Wang V and Kawazoe Y 2016 *J. Mater. Chem. C* **4** 9613